

Chitosan/Fe Doped Hydroxyapatite Scaffold for Bone Tissue Regeneration

Maskanati M¹, Motiee F¹, Aghabozorgb H¹, Masoumeh Meskinfam^{2,3*}

¹Department of chemistry, North Tehouran Branch, Islamic Azad University, Tehouran, Iran

²Department of chemistry, Lahijan branch, Islamic Azad University, Lahijan, Iran

³Department of Chemistry, Materials and Chemical Engineering "G. Natta" Politecnico di Milano, Milano, Italy

Article History:

Submitted: 02.07.2021

Accepted: 16.07.2021

Published: 23.07.2021

ABSTRACT

Porous scaffolds containing calcium phosphate phase similar to bone apatite with appropriate cell interaction is a promising alternative to autologous and heterologous bone grafts. Chitosan (CS)/Fe doped hydroxyapatite (Fe-HAp) are here investigated as scaffold for bone tissue regeneration. Formation of scaffolds carried out by introducing Fe doped apatite nanoparticles into the chitosan solution via freeze-drying method to develop a bio-integrable matrix with desirable geometries to support cell adhesion, growth and anchorage onto the pore walls of the CS scaffolds. Scanning electron microscopy (SEM), Energy-dispersive X-ray spectroscopy (EDS), Fourier Transform Infrared spectroscopy (FT-IR) and X-Ray Diffraction (XRD) analysis of Fe substituted calcium phosphate powders showed the formation of spherical nano particles of Fe doped hydroxyapatite (Fe-nHAp) with uniform size distribution and magnetic

property (saturation magnetization (Ms) and coercivity, about 0.25 emu/g and 50 Oe, respectively). Scaffolds morphological characterization confirmed that immersion time of Fe ions for being doped in apatite lattice has effect on the morphology of distributed Fe-HAp particles through the CS porous structure. Fe doped apatite also affected the CS scaffold cytocompatibility, providing more suitable surface for cell spreading, attachment and proliferation. This scaffold can be a good candidate for bone tissue regeneration applications considering the obtained results.

Keywords: Chitosan, Hydroxyapatite, Magnetic nanoparticles, Bone, Tissue engineering

***Correspondence:** Masoumeh Meskinfam, Department of Chemistry, Lahijan branch, Islamic Azad University, Lahijan, Iran, E-mail: meskinfam@gmail.com

INTRODUCTION

In recent years, a lot of patients suffering of bone defects caused by trauma, tumor or diseases and a large number of investigations are in progress to develop new materials (Kim CW, *et al.*, 2008; Shi X, *et al.*, 2007) and techniques (Song K, *et al.*, 2004; Torigoe I, *et al.*, 2007) for bone tissue regeneration. Nowadays, autografts, allografts and demineralized heterologous bone are used as clinical therapies for bone regeneration. Autografts are good choice due to their osteoconductivity and non-immunogenicity, (Schouroeder JE and Mosheiff R, 2011) while their usage is limited by donor shortage and donor site morbidity. The drawbacks of using allografts are the risk of immunological problems and disease transmission (Shalumon K, *et al.*, 2009). Therefore, the alternative source combining life science and engineering principles for developing biological substitutes to maintain, restore, or improve the function of tissue, 8, 9 can be a good solution for bone defect reconstruction (Rose FR, Oreffo RO, 2002; Livingston T, *et al.*, 2003; Takahashi Y, *et al.*, 2005).

Suitable scaffold for bone regeneration should possess some important characteristics such as having proper surface chemistry for supporting the cell adhesion, proliferation, migration and growth, in addition to highly interconnected pores with adequate size for promotion of cell migration and nutrient distribution (Tetteh G, *et al.*, 2014). Porous scaffolds containing biodegradable biomimetic materials, which provide both temporary mechanical support and a site for tissue development, can be a good candidate for bone tissue engineering (Meskinfam M, *et al.*, 2018; Yang X, 2017). Additionally, the porous scaffold plays an important role in the formation of new bone with desired shapes as well as manipulation of the osteoblasts functions (Berger J, *et al.*, 2004; Heidari F, *et al.*, 2018).

Both natural and synthetic polymers can be used for bone tissue

regeneration as they have ability to be processed into three-dimensional (3D) structures (Ge S, *et al.*, 2012). Different kind of synthetic biodegradable polymers such as polyurethanes (Yang X, 2017; Tanzi MC, *et al.*, 2003) poly (lactide-co-glycolide) (Kim SS, *et al.*, 2006; Nie H, Wang CH, 2007) poly (α -hydroxyesters) (Ren J, *et al.*, 2007) and polyorthoesters (Ren J, *et al.*, 2007) have been applied for bone tissue regeneration. It is noticed that chitosan (Sekharan S, *et al.*, 2016) gelatin (Khan MN, *et al.*, 2021) Collagen (Oliveira SM, *et al.*, 2010) alginate (Valente J, *et al.*, 2012) and hyaluronic acid (Kim J, *et al.*, 2007) are the most promising natural polymers for bone tissue engineering purpose. Chitosan is a polysaccharide which can be obtained by the deacetylation of chitin. Chitosan can substitute GlycosAminoGlycan (GAGs) in bone extracellular matrix (ECM) due to its solubility in aqueous solution. Chitosan is a suitable choice for tissue engineering, drug delivery and regenerative medicine due to its excellent biodegradability and biocompatibility. As chitosan is a flexible polymer, it cannot fulfil the natural bone mechanical properties requirement (Park KH, *et al.*, 2017; Prajateljista E, *et al.*, 2015). The best way for improving the mechanical properties of the natural polymer based scaffolds such as chitosan is reinforcement of them with introduction of inorganic particles into their structure (Yang X, 2017; Suren UP, *et al.*, 2016) and there are some attempts that showed chitosan/hydroxyapatite (CS/HA) scaffolds are suitable for bone regeneration. Hydroxyapatite (HAp) by $\text{Ca}_{10}(\text{PO}_4)_6(\text{OH})_2$ formula has excellent biocompatibility, osteoconductivity and structural similarity to natural bone minerals and can be a good choice for reinforcement of the natural polymer based scaffolds (Cai B, *et al.*, 2016; Azhar FF, *et al.*, 2014; Nazeer MA, *et al.*, 2017). Formation of calcium phosphate interface similar to bone apatite on the surface of synthetic material is an important requirement for scaffold to show the bone bonding behavior (Hanawa T and Davies J, 1991; Hench LL, 1991). So, existence of apatite-like layer

on the scaffold will let us to expect positive biological response from the host tissues and showing a bioactive behavior after implantation. Dissolution of nano-hydroxyapatite (nHAp) in the human body is very low after implantation whereas the dissolution rate is a key factor for bioactivity and tissue regeneration success (Reis R, *et al.*, 1997). One promising approach for nHAp biological properties improvement is the ionic substitutions in its lattice structure. The osteogenic properties of nHAp can be improved by the substitution of Fe ions into its structure (Park SY, *et al.*, 2017). Fe as an essential nutrient for all living organisms except certain bacteria has key role in vital metabolic processes, such as DNA synthesis, oxygen and electron transport (Duggan C, *et al.*, 2016). Drug delivery, magnetic resonance imaging, tissue engineering and magnetic hyperthermia are some application of Fe-nHAp (Gloria A, *et al.*, 2013; Iwasaki T, *et al.*, 2013; Chandra VS, *et al.*, 2012; Sneha M and Sundaram NM, 2015). Researches showed that Fe ions have a positive effect on bone health (Maurer J, *et al.*, 2005). Presence of Fe ions in HAp structure can enhance the osteoblast adhesion and growth to promote bone regeneration (Panseri S, *et al.*, 2012). Different methods such as ion exchange (Zilm ME, *et al.*, 2014), pickering emulsion, (Iafisco M, *et al.*, 2013) hydrothermal (Gloria A, *et al.*, 2013) and wet chemistry (Radha G, *et al.*, 2019) have been applied for synthesis of Fe substituted HA which led to products with different magnetic properties and enhanced cell response for better bone bonding ability (Gloria A, *et al.*, 2013).

In the present study, chitosan based scaffold containing Ca_{10-x}Fe_x(PO₄)₆(OH)₂, considering the mentioned advantages of each components were performed which this design has not been reported elsewhere. Physical, chemical and biological characterization of scaffolds was also carried out.

MATERIALS AND METHODS

Nano hydroxyapatite (nHAp) preparation

The precipitation method was applied to synthesize the nHAp powders. For this purpose, the solution of 0.096 M (NH₄)₂HPO₄ (reagent grade, Merck) was added drop-wise (2.5-5 ml/min), into 0.16 M Ca(NO₃)₂ (reagent grade, Merck) solution under stirring at 60°C to give the desired atomic ratio of Ca/P=1.67. Meanwhile, dilute NH₄OH (reagent grade, Merck) solution was used for adjusting the pH of the solution to about 10. Then, the solution was poured into a sealed container and was vigorously stirred and aged for about 6 hours. The solution was filtered, washed and dried at 100°C overnight.

Preparation of iron substituted hydroxyapatite (Fe-nHAp)

A simple ion exchange procedure was used to achieve Fe substituted nHAp, in which calcium would be substituted by iron in the HAp crystal lattice. Briefly, the nHAp powder was soaked in a solution of FeCl₃.6H₂O 40%w/v (97 wt%, Sigma-Aldrich) with a ratio of nHAp/solution=0.5 g/100 ml, under stirring for a desired time (1, 6 and 12 hours). The obtained solids were filtered and washed thoroughly by distilled water. The powder (Fe-nHAp) was then dried overnight at ambient temperature and grinded by a mortar and a pestle.

Preparation of the scaffolds CS/Fe-nHAp

CS/Fe-nHAp scaffolds preparation steps is presented in Figure 1, schematically. For this purpose, CS powder (medium molecular weight and a degree of deacetylation of 85%) was provided from Sigma-Aldrich and dissolved in 1% of acetic acid (Sigma-Aldrich) solution, led to a concentration of 2%. A transparent solution was obtained under stirring for 4 hours. The required amount of prepared Fe-nHAp nanoparticles was added to CS solution to give a desired percentage of nano inorganic particles in scaffolds which are mentioned in Table 1. The solution was then stirred for 10-20 hours to obtain a uniform mixture. The obtained mixture was poured into a mould with a diameter and a thickness of 12 and 2 mm, respectively, followed by freezing at -20°C for 12 hours (Figure 2). A freeze-drying ma-

chine (CHOURist, 1-4 LD model) was used to dry the above-mentioned solidified mixtures at -35°C for 36 hour. The obtained CS/Fe-nHAp scaffolds were washed with 50 ml NaOH (Merck, 10.0 wt%) and deionized water and then dried at 60°C. For evaluation of the Fe-nHAp effect on the physical and biological properties of the samples, CS and CS/nHAp scaffolds were prepared by omitting the Fe-nHAp and Fe soaking part of synthesis, respectively.

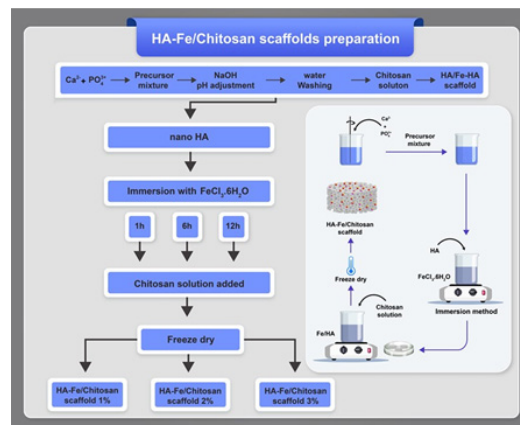


Figure 1: Schematic diagram of CS/Fe-nHAp scaffolds fabrication

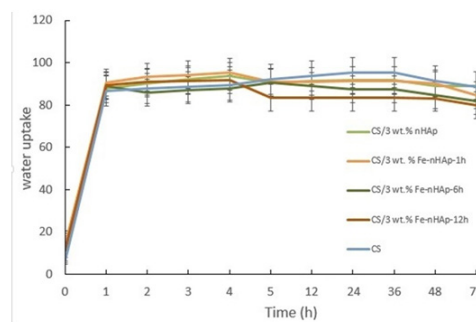


Figure 2: Water uptake kinetics for CS, CS/3 wt% HAp, CS/3 wt% Fe-nHAp-1h, CS/3 wt% Fe-nHAp-6h and CS/3 wt% Fe-nHAp-12h

Table 1: The summarized preparation condition of the scaffolds

Sample name	nHAp (Wt%)	Fe-nHAp (Wt%)	Soaking time (hr)
CS	-	-	-
CS/1% HAp	1	-	-
CS/2% HAp	2	-	-
CS/3% HAp	3	-	-
CS/1% Fe-HAp-1h	-	1	1
CS/1% Fe-HAp-6h	-	1	6
CS/1% Fe-HAp-12h	-	1	12
CS/2% Fe-HAp-1h	-	2	1
CS/2% Fe-HAp-6h	-	2	6
CS/2% Fe-HAp-12h	-	2	12
CS/3% Fe-HAp-1h	-	3	1
CS/3% Fe-HAp-6h	-	3	6
CS/3% Fe-HAp-12h	-	3	12

Note: Fe-nHAp: Fe doped hydroxyapatite

Chemicophysical characterization

As physical characterization, water uptake characteristic of CS, CS with 3% HAp and Fe-Ap samples (2 × 2 cm, n=4), were evaluated by immersion of each specimen in 500 µl of phosphate buffer saline (PBS) with pH

of 7.4 at 37°C. To obtain more clear graphs, samples with higher content of inorganic particles were considered. At each time point (t=15 min, 30 min, 1, 2, 3, 6, 24 hours and every hour until reaching to the absorption plateau), samples were blotted with laboratory paper to remove excess liquid and weighed. Swelling ratio, SW (%), was calculated according to the (Equation 1)

$$SW(\%) = (W_t - W_0) / W_0 \times 100 \quad (1)$$

Where W₀ is the dry weight and W_t is the wet weight at each time point.

FT-IR, XRD and EDAX analyses have been applied for chemical characterization. The functional groups of calcium phosphate phase and Fe substituted powders were evaluated by Fourier Transform Infrared spectroscopy (FT-IR, Shimadzu 8400 s). Samples for analysis have been prepared as KBr pellet. For this reason, 2-3 mg of calcium phosphate powders were mixed with 98 mg of dried KBr powder, homogenized, finely pulverized, and put into a pellet-forming die to obtain transparent pellets for recording FT-IR spectra over the range of 400-4000 cm⁻¹.

The crystal structure of the calcium phosphate and Fe substituted powders was investigated by X-ray diffraction (XRD, X'Pert PRO MPD PANalytical Company). Inorganic powders were smoothen and placed in the sample holder and XRD patterns were recorded at 2 θ ranging from 20 to 60 degrees.

Elemental analysis of calcium phosphate phase and Fe doped powders was performed by energy dispersive X-ray spectroscopy (EDAX EDS Silicon Drift 2017).

Magnetic property

Magnetization measurement of Fe substituted HAp has been performed at room temperature by a vibrating sample magnetometer (VSM) with magnetic field of 0-10 Koe (Magnetic Daghigh Daneshpajouh Co., Iran)

Morphological characterization

The morphology of the prepared nHAp, Fe-nHAp, CS, CS-HAp and CS-Fe-nHAp scaffolds were analysed using SEM imaging (Serontechnologies-AIS2100) with 25 kV of accelerating voltage. The samples were coated in a sputtering device (Polaron SC7640) for better conductivity and resulting high quality SEM imaging.

In vitro cytocompatibility tests

Samples of CS, CS/1% HAp and CS/Fe-nHAp (1% and 3% after 1 and 12 hour immersion) (0.5 × 0.5 cm, n=3) were placed in a flat-bottom 24 multi well culture plate, treated with UV light at both side for 30 minutes to be sterilized. Fibroblast L929 cells (cell density=104 cells/well) were seeded on each scaffold and cells cultured on Tissue Culture Polystyrene (TCPS) considered as control. The samples were incubated up to 7 days of culture at 37°C and 5% CO₂. The attached and grown viable cells on the scaffolds were evaluated by MTT (3-(4, 5-dimethylthiazol-2-yl)-2,5-diphenyltetrazolium bromide) colorimetric assay at 3, 5, 7 days post seeding. For assessing the cell viability at each time point, 100 μl MTT solution (5 mg/ml in PBS) was added to each well and incubated for 4 hour at 37°C. Then, the upper solvent (MTT solution) was removed and 1 ml of 10% sodium dodecyl sulfate (SDS, Sigma) in 0.01 N HCl added to the solution to dissolve the formazan crystals at 37°C. At the end, the absorbance of dissolved formazan for each sample was measured at 570 nm using a microplate reader (ELISA reader, ELX808, BioTek). The absorption value of the MTT solution alone was subtracted from the values related to seeded samples and control.

The scaffolds of CS/1% HAp and Chitosan/Fe-nHAp 1 and 3% after 12 hour immersion were observed by SEM (Serontechnologies-AIS2100), to evaluate fibroblast cells morphology, distribution and attachment on the scaffolds surface. Scaffolds at time points 3 and 7 days were washed with PBS, fixed in 2.5% glutaraldehyde solution for 1 hour, dehydrated thorough a series of ethyl alcohol solutions in distilled water (from 10 to

100% ethyl alcohol) and air dried. Samples were gold sputter coated and observed at 25 kV, at different magnifications.

Statistical analysis

The obtained data in this study were reported in the form of mean ± standard deviation values and were analysed *via* Student t-test with significance level p=0.05. SPSS software (v 17.0; IBM New York, NY, USA) was used for statistical analysis.

RESULTS AND DISCUSSION

Scaffold design

Development of new materials such as scaffolds for tissue regeneration has attracted a great attention because there is limitation in availability of human tissues for transplantation, regeneration and repair of organs. Scaffolds for bone regeneration should fulfil different requirements to provide a suitable bone-engineered tissue. The presence of interconnected pores with appropriate size to provide support for cell infiltration, adhesion and proliferation is the most important property of scaffolds. Chitosan is a natural polysaccharide with a suitable shock absorbing capacity and have an ability to substitute glycosaminoglycan in bone extracellular matrix (ECM). Formation of 3D porous scaffolds of chitosan with interconnected pores as well as its good biocompatibility and biodegradability has been made it as a suitable choice for tissue engineering (Singh YP, *et al.*, 2015). Another primary requirement for applicable scaffold in hard tissues is load bearing capability and high mechanical strength (Rahman MS, *et al.*, 2019; Yang J, *et al.*, 2014). As chitosan is a flexible polymer, it cannot fulfil mechanical properties of bone. Therefore, several attempts have been performed for improvement of mechanical strength of chitosan scaffolds such as introducing inorganic calcium phosphate particles (Nazeer MA, *et al.*, 2017; Singh YP, *et al.*, 2015). Several researches (Hench LL, 1991; Reis R, *et al.*, 1997) have claimed that the formation of calcium phosphate on the surface of synthetic materials lead to the growth of cells on them which is an important requirement for exhibiting the behavior of a bone-bonding. In addition, the presence of apatite-like layer on the scaffold will cause the positive biological response from the host tissues which lead to show a bioactive behavior after implantation (Reis R, *et al.*, 1997). Some studies (Baxter LC, *et al.*, 2002; Tagaya M, *et al.*, 2011) have shown the influence of different calcium phosphates phases such as beta tricalcium phosphate and hydroxyapatite (Baxter LC, *et al.*, 2002) or hydroxyapatite nano crystals (Zilm ME, *et al.*, 2014) on fibroblast cells morphology, attachment and proliferation. It has been shown that ionic substitutions such as Fe ions in nHAp lattice structure can improve its biological and osteogenic properties (Park SY, *et al.*, 2017). Heidari *et al.* used natural HA, extracted from bone, and also natural CS, prepared from shourimp shells, followed by in situ precipitation of magnetic nanoparticles, Fe₃O₄ in the CS/HA matrix to prepare suitable composites for bone tissue engineering. Their main focus was on evaluation of mechanical and cytocompatibility properties of composites (Heidari F, *et al.*, 2018; Heidari F, *et al.*, 2016).

In the present study as it has been shown in Fig.1, a spongy porous CS-Fe-HAp scaffolds with pore diameter about 30 μm were synthesized *via* a simple method to develop a biointegrable matrix with desirable geometries to support cell adhesion, growth and anchorage onto the pore walls of the CS, thanks to presence of the Fe ion in structure of osteoinductive and osteoconductive HAp.

Water uptake

Scaffolds ability for retaining water is an important factor to evaluate its efficacy for tissue engineering. It has been shown that swelling properties of scaffolds have significantly influence on cells adhesion, growth and differentiation (Li Z, *et al.*, 2005). In the water uptake (SW%) tests (Figure 2), different water absorption kinetics up to 72 hours can be observed. Chitosan is a hydrophilic polymer with a high water uptake capability due to the presence of free ammine groups in its structure.

All samples showed the highest water affinity, reaching to maximum swelling degree in 1 hour. In fact, the plateau was reached very fast (i.e. after 1 hour) for all samples. It seems that introducing nHAp in chitosan scaffold and also Fe ions doping in the apatite lattice structure have not effect on water uptake characteristic of prepared samples. It is clear that after reaching the plateau, no statistically differences in SW% were detected up to 72 hours of incubation for all samples.

FTIR analysis

The functional groups of pure HAp and FeHAp powders after 1, 6, and 12 hour immersion times were evaluated by Fourier transform infrared spectroscopy. The FTIR spectra of samples (Figure 3) showed the presence of functional groups attributed to hydroxyapatite. The existing peaks at ~560-600 cm⁻¹, 960 cm⁻¹ and 1030 cm⁻¹ can be related to out-of-plane bending, symmetrical stretching and asymmetric stretching of phosphate groups, respectively. There are peaks at about 1650 cm⁻¹ and 1470 cm⁻¹, which can be corresponded to carbonate peaks. Besides that, a broad band at 3566 cm⁻¹ can be attributed to the main vibration of symmetrical stretching of OH. The obtained spectra of the samples are in good agreement with our previous work (Yang X, 2017; Aslani M, *et al.*, 2017). It can be seen that there is no considerable difference between the spectra of the HAp and FeHAp powders. This implies that the FeHAp and pure HA have similar functional groups. However, the splitting of the band in range of 450 cm⁻¹-650 cm⁻¹ is decreased by addition of Fe ions doping in substitution of Ca which is consistent with the result reported by Kamal *et al.* (Gloria A, *et al.*, 2013). In addition, the hydroxyl peak intensity at 3500 cm⁻¹, increases as the Fe is doped to the HAp lattice structure.

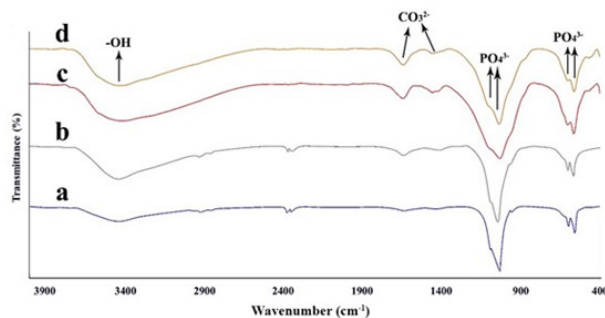


Figure 3: The FTIR spectra of the (a) HAp, (b) FeHAp-1h, (c) FeHAp-6h, and (d) FeHAp-12h

XRD analysis

The XRD patterns of Fe-doped HAp with different soaking times (1, 6, and 12 hour) comparing to HAp pattern is presented (Figure 4). All the diffraction peaks in XRD patterns can be assigned to monophasic, low crystalline hydroxyapatite which is consistent with the peaks of the HAp (JCPDS card No.9-432). In patterns, obvious diffraction peaks can be seen at 25.9°, 28.2°, 29°, 31.9°, 32.9°, 34.1°, 39.9°, 46.8°, 49.5°, and 53.1° which are corresponded to 002, 102, 210, 211, 300, 202, 310, 222, 213, and 004 planes

of HAp, respectively. In all Fe ions doped HAp samples, no diffraction peaks appeared other than those attributed to HAp. In addition, no significant shifting of peak positions and no obvious changing in relative peak intensities after ion exchange, regardless of soaking time were observed in XRD patterns. Therefore, it seems that the ion exchange process does not change or modify the structure of HAp. All samples showed the broadened peaks, indicating the nano size and low crystalline structure of apatite (Yang X, 2017) As it can be seen in the Fe-HAp samples, increasing the time of soaking lead to more broadening the characteristic peaks of apatite.

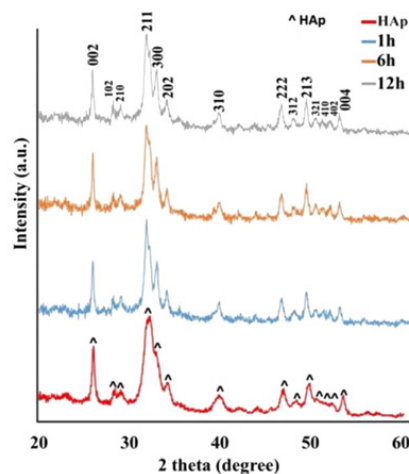


Figure 4: XRD patterns of HAp, FeHAp-1h, FeHAp-6h and FeHAp-12h

EDAX elemental analysis

Elemental analysis of inorganic nano particles was performed by EDAX. The EDAX spectra of HAp (Figure 5a) showed the presence of Ca, P and O, whereas in Fe doped HAp powders after 1 and 12 hour soaking (Figures 5b and 5c), Fe is present in addition to Ca, P, and O elements. Fe³⁺ ions are not so thermodynamically stable in aqueous environment at room temperature. Therefore, there would be an enough driving force for Fe³⁺ ions to interact with the HA lattice and it can be said that Fe is substituted in the HAp structure. EDAX analysis results for the samples are presented in Table 2. Furthermore, the Ca/P ratios of the HAp as well as FeHAp were calculated. It is clear that the Fe weight percent for FeHAp-12 hr is higher than that of FeHAp-1 hour sample, which proves more substitution of Fe ions by increasing the immersion time during the synthesis of FeHAp powders. Moreover, the Ca/P atomic ratio was 1.7, 0.9 and 0.83 for HAp, FeHAp-1 h and FeHAp-12 h samples, respectively. As it can be seen, the Ca/P ratio of Fe HAp samples is lower than pure HAp. If a one-for-one substitution has been occurred between iron and calcium in FeHAp, then it is expected that Ca/P ratio be equal to HAp. This decreasing in ratio can be derived from this fact that divalent ion (Ca) replaced by trivalent (Fe) ones. There may be calcium vacancies be formed to compensate the lattice charge imbalance which resulted from iron substitution.

Table 2: EDAX (Energy dispersive x-ray spectroscopy) analysis results for the samples

Sample	Element							
	Fe		Ca		P		Ca/P	
	Wt%	Atom%	Wt%	Atom%	Wt%	Atom%	Wt/Wt	Atom/Atom
HAp	-	-	51.6	35.7	23.3	20.8	2.2	1.7
FeHAp-1h	14.7	6.4	23.2	14.1	19.7	15.5	1.2	0.9
FeHAp-12h	17.4	8.1	24.4	15.8	22.8	19	1.07	0.83

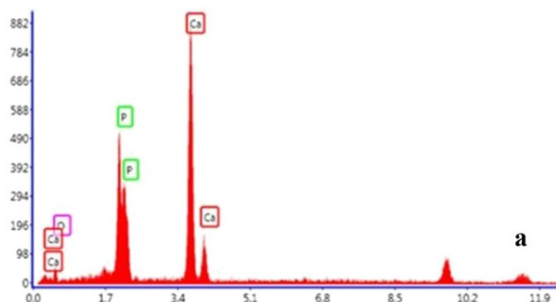


Figure 5(a): EDAX elemental analysis of Hap

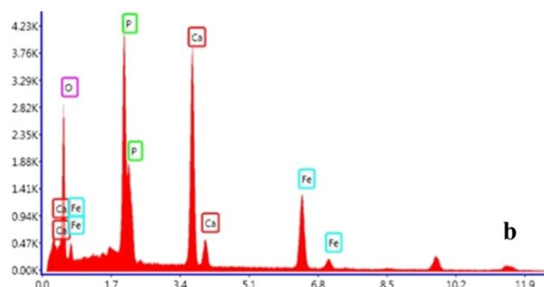


Figure 5(b): EDAX elemental analysis of FeHAp-1h

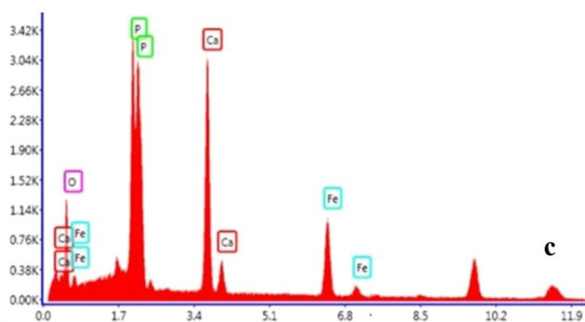


Figure 5(c): FeHAp-12h powder samples

Magnetic properties

VSM test was performed to evaluate the magnetic properties of FeHAp at ambient temperature in a field of 10 Koe (Figure 6). It can be seen that all FeHAp samples showed almost paramagnetic properties, which is clear from their positive slope of the corresponding magnetization-magnetic field curve. Although iron doping in all FeHAp samples led to magnetic properties, there was no specific pattern between soaking time and magnetic properties so that FeHAp-12h showed lower Ms than FeHAp-6h which is against of this expectation that more iron substitution may lead to higher saturation magnetization.

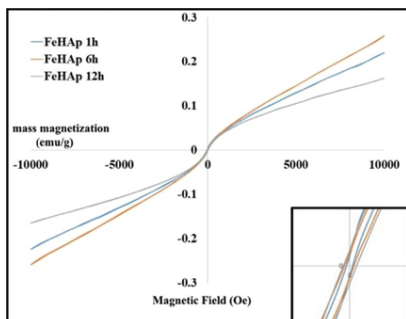


Figure 6: Magnetization-magnetic field FeHAp samples with different time of soaking

Morphological characterization

The pore shapes, interconnectivity and distribution in scaffolds as well as morphology of inorganic particles were evaluated by SEM. The synthesized HAp powders (Figure 7a) consisted of tiny agglomerated particles around 60 to 80 nm, while the Fe HAp powder (Figure 7b) showed spherical particles with more uniform size distribution around 60 nm. CS scaffold (Figure 7c) presented more homogenous pore structure with about 20 μm in size compare to CS/HAp, and CS/3% FeHAp-6h samples (Figures 7d and 7e). It seems that introducing HA in the structure of CS scaffold has led to formation of more closed pores (Fig.7d) while addition of magnetic FeHAp particles have influence on the scaffolds structure thorough reducing the pore size (Figure 7e) which may be due to well-precipitation of Fe into the CS matrix thorough freeze-drying technique. There are several agglomerated nano-sized HAp and FeHAp particles, distributed in the CS matrix (Figures 7d and 7e) which lead to a rough surface to provide more surface area and thus enough sites for cells viability. Representative SEM images of CS/3% FeHAp samples at different soaking time (Figures 8 a-8c) showed the effect of immersion time in Fe ions solution on the morphology of FeHAp nanoparticles distributed in the CS matrix. 1 hour soaking time (Figure 8a) led to formation of FeHAp particles distributed almost uniformly on the surface and inner pore walls of scaffold with less agglomeration compare to 6 hour immersion time (Figure 8b). Increasing the soaking time to 12 hours caused the formation of plates like FeHAp crystals with length and width about 12 and 4 μm, respectively. It seems that soaking time has effect on the way of nano inorganic particles precipitation in the CS matrix during freeze drying and led to formation of FeHAp particles with different morphology into the CS scaffolds.

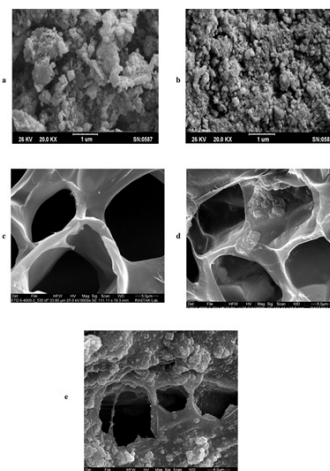


Figure 7: SEM micrographs of (a) HAp nano particles (b) FeHAp nano particles, (c) CS, (d) CS/ 1 % HAp, and (e) CS/ 3 % FeHAp-6h samples

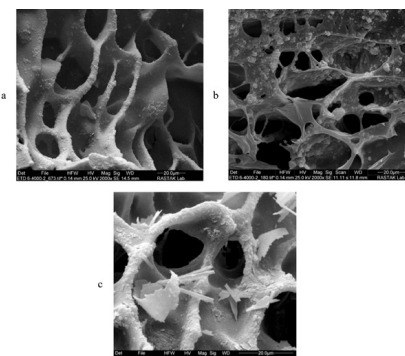


Figure 8: SEM micrographs of (a) CS/3% FeHAp-1h, (b) CS/3% FeHAp-6h, and (c) CS/3% FeHAp-12h

In vitro cytocompatibility test

Fibroblast L929 cells were cultured on CS, CS/HAp and CS/Fe-HAp samples up to 7 days, using TCPS as control. All samples showed higher number of the viable cells by passing the cell culture time (Figure 9). As it can be seen no significant difference is observable for cell viability of all samples after 3 and 5 days of culture ($p > 0.05$) whereas after 7 days the difference is significant ($p < 0.05$). Different literature evaluated the effect of introducing Fe ions in HAp structure on cell proliferation and attachment. Chandra *et al.* (Gloria A, *et al.*, 2013 synthesized the Fe-doped natural HAp through a combination of microwave and hydrothermal techniques and found out that presence of the Fe³⁺ ions led to a higher bioactivity and cell proliferation using MG63 osteo-sarcoma cells. Panserie S, *et al.*, 2012 evaluated the FeHAp nanoparticles cytocompatibility using Saos-2 human osteoblast-like cells which showed good cell proliferation, morphology and attachment, compared to pure HAp nanoparticles. Therefore, it seems that presence of Fe ions in apatite structure enhance the cell viability which it is also consistent with our results for CS/3% Fe-HAp-12h sample. This sample has the more apatite and Fe ions in its structure compare to other samples and showed the cell viability close to TCPS after 7 days of culture with no significant difference ($p > 0.05$, Figure 9). It seems that the presence of 3% apatite in CS/3% Fe-HAp-1h has the same effect of Fe ions presence in CS/1% Fe-HAp-12h on biological response so that there is no significant difference for cell viability of these samples after 7 days culture ($p > 0.05$, Figure 9). The cell viability of CS/1% Fe-HAp-1h after 7 days was close to CS/1% HAp ($p > 0.05$) and it seems that the low quantity of Fe ion presence in apatite structure did not have effect on cell proliferation.

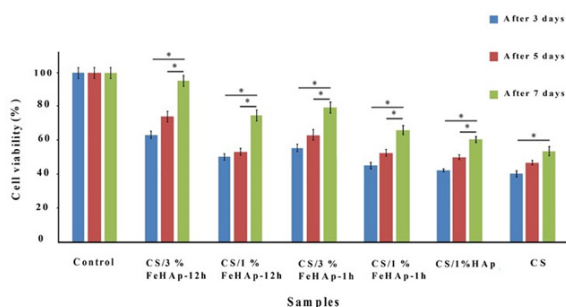


Figure 9: Relative cell viability of fibroblast L929 cells cultured on CS, CS/1% HAp, CS/1, 3% Fe-HAp-1h and CS/1, 3% Fe-HAp-12h at the three considered time points. Note: *= $p < 0.05$

The morphology of the attached cells on the CS/1% HAp, CS/1% Fe-HAp-12h and CS/3% Fe-HAp-12h scaffolds at different culture times were observed by SEM (Figure 10). By increasing culture time, cell attachment improved on the surface of all scaffolds (Figures 10c and 10d, Figures 10g and 10h, Figures 10k and 10l). In CS/1% HAp, fewer cells were attached on the surface and the cells were not fully stretched (Figures 10a-10d). In the Fe doped HAp samples (Figures 10c-10l), long cytoplasmic branches were formed by cells on samples, in which the cells interacted with pore walls. This can be because of the surface biomineralization that provided appropriate attachment sites for fibroblast cells and maybe due to improvement of apatite dissolution through substitution of Fe ions in its structure 34 which may cause the release of Ca²⁺ and PO₄³⁻ ions, Ca-P precipitation and promotion of protein absorption and finally better cell adhesion and proliferation. In addition, fibroblast cells became well spread after 7 days, better adhering onto the CS/3 wt% FeHAp-12h sample (Figures 10k-10l). These results demonstrate that CS/Fe-HAp samples provided desirable surface to support fibroblast cells adherence, spreading and proliferation compare to CS/HAp sample and the quantity of Fe doped HAp has a positive effect on cell response.

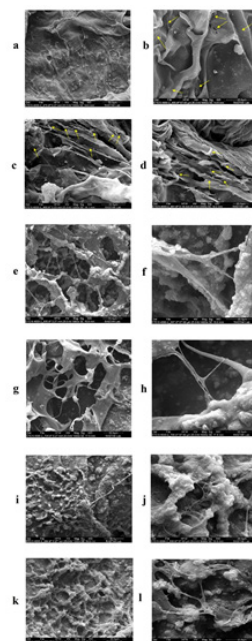


Figure 10: SEM micrographs of (a,b) CS/1% HAp after 3 days; (c,d) CS/1% HAp after 7 days; (e,f) CS/1% Fe-HAp-12h after 3 days; (g,h) CS/1% Fe-HAp-12h after 7 days; (i,j) CS/3% Fe-HAp-12h after 3 days, and (k,l) CS/3% Fe-HAp-12h after 7 days culture by fibroblast L929 cells. Yellow arrows represents the cells spread on samples surface. Scale bar: 50 μ m (a, c, e, g, i and k), 20 μ m (b, d, f, h, j and l)

CONCLUSION

Introducing the nano hydroxy apatite on the surface of scaffolds can be a useful method to develop suitable materials for bone tissue regeneration, regarding to their physical, chemical and morphological properties and ability to promote cells adhesion, spreading and proliferation. In this study, ion exchange procedure was used to prepare FeHAp powders with magnetic properties. Introducing these nano inorganic particles into the CS structure led to formation of scaffolds which presented improved fibroblast cell adhesion and proliferation. Further improvements of fibroblast cells performance on CS/FeHAp scaffold can be achieved by doping more Fe ions in apatite structure and *in vitro* cell culture under dynamic condition such as perfusion chambers, and bioreactors.

ACKNOWLEDGMENT

This project was financially supported by North Tehouran branch, Islamic Azad University.

REFERENCES

1. Kim CW, Talac R, Lu L, Moore MJ, Currier BL, Yaszemski MJ. Characterization of porous injectable poly-(propylene fumarate)-based bone graft substitute. *J Biomed Mater Res A*. 2008; 85(4): 1114-1119.
2. Shi X, Sitharaman B, Pham QP, Liang F, Wu K, Billups WE, *et al.* Fabrication of porous ultra-short single-walled carbon nanotube nanocomposite scaffolds for bone tissue engineering. *J Biomaterials*. 2007; 28(28): 4078-4090.
3. Song K, Liu T, Cui Z, Li X, Ma X. Three-dimensional fabrication of engineered bone with human bio-derived bone scaffolds in a rotating wall vessel bioreactor. *J Biomed Mater Res A*. 2008; 86(2): 323-332.
4. Torigoe I, Sotome S, Tsuchiya A, Yoshii T, Takahashi M, Kawabata S, Shinomiya K. Novel cell seeding system into a porous scaffold using a modified low-pressure method to enhance cell seeding efficiency and bone formation. *Cell Transplant*. 2007; 16(7): 729-739.

5. Schroeder JE, Mosheiff R. Tissue engineering approaches for bone repair: Concepts and evidence. *Injury*. 2011; 42: 609-613.
6. Shalumon K, Binulal N, Selvamurugan N, Nair S, Menon D, Furuike T, *et al.* Electrospinning of carboxymethyl chitin/poly (vinyl alcohol) nanofibrous scaffolds for tissue engineering applications. *Carbohydr Polym*. 2009; 77(4): 863-869.
7. Rose FR, Oreffo RO. Bone tissue engineering: Hope vs. hype. *Biochem Biophys Res Commun*. 2002; 292(1): 1-7.
8. Livingston T, Gordon S, Archambault M, Kadiyala S, McIntosh K, Smith A, *et al.* Mesenchymal stem cells combined with biphasic calcium phosphate ceramics promote bone regeneration. *J Mater Sci: Mater*. 2003; 14(3): 211-218.
9. Takahashi Y, Yamamoto M, Tabata Y. Osteogenic differentiation of mesenchymal stem cells in biodegradable sponges composed of gelatin and β -tricalcium phosphate. *Biomaterials*. 2005; 26(17): 3587-3596.
10. Tetteh G, Khan A, Smith RMD, Reilly G, Rehman I. Electrospun polyurethane/hydroxyapatite bioactive Scaffolds for bone tissue engineering: The role of solvent and hydroxyapatite particles. *J Mech Behav Biomed Mater*. 2014; 39: 95-110.
11. Meskinfam M, Bertoldi S, Albanese N, Cerri A, Tanzi M C, Imani R, *et al.* Polyurethane foam/nano hydroxyapatite composite as a suitable scaffold for bone tissue regeneration. *Mater Sci Eng C*. 2018; 82: 130-140.
12. Yang X. Hydroxyapatite: Design with nature. *Tissue Eng*. 2017: 141-165.
13. Pistone A, Iannazzo D, Panseri S, Montesi M, Tampieri A, Galvagno S. Hydroxyapatite-magnetite-MWCNT nanocomposite as a biocompatible multifunctional drug delivery system for bone tissue engineering. *Nanotechnology*. 2014; 25(42): 425701.
14. Berger J, Reist M, Mayer JM, Felt O, Peppas N, Gurny R. Structure and interactions in covalently and ionically crosslinked chitosan hydrogels for biomedical applications. *Eur J Pharm Biopharm*. 2004; 57(1): 19-34.
15. Heidari F, Razavi M, Bahrololoom ME, Yazdimamaghani M, Tahriri M, Kotturi H, *et al.* Evaluation of the mechanical properties, in vitro biodegradability and cytocompatibility of natural chitosan/hydroxyapatite/nano-Fe₃O₄ composite. *Ceram Int*. 2018; 44(1): 275-281.
16. Ge S, Zhao N, Wang L, Yu M, Liu H, Song A, *et al.* Bone repair by periodontal ligament stem cellseeded nanohydroxyapatite-chitosan scaffold. *Int J Nanomedicine*. 2012; 7: 5405-414.
17. Tanzi MC, Fare S, Petrini P, Tanini A, Piscitelli E, Zecchi-Orlandini S, *et al.* Cytocompatibility of polyurethane foams as biointegrable matrices for the preparation of scaffolds for bone reconstruction. *J Appl Biomater Funct Mater*. 2003; 1(1): 58-66.
18. Kim SS, Park MS, Gwak SJ, Choi CY, Kim BS. Accelerated bonelike apatite growth on porous polymer/ceramic composite scaffolds in vitro. *Tissue Eng*. 2006; 12(10) 2997-3006.
19. Nie H, Wang CH. Fabrication and characterization of PLGA/HAp composite scaffolds for delivery of BMP-2 plasmid DNA. *J Control Release*. 2007; 120(2): 111-121.
20. Ren J, Ren T, Zhao P, Huang Y, Pan K. Repair of mandibular defects using MSCs-seeded biodegradable polyester porous scaffolds. *J Biomater Sci Polym Ed*. 2007; 18(5): 505-517.
21. Sekharan S, Saleth LR, Selvamurugan N. Chitosan based biocomposite scaffolds for bone tissue engineering. *Int J Biol Macromol*. 2016; 93: 1354-1365.
22. Khan MN, Islam JM, Khan MA. Fabrication and characterization of gelatin-based biocompatible porous composite scaffold for bone tissue engineering.
23. *J Biomed Mater Res*. 2021; 100A(11): 3020-3028.
24. Oliveira SM, Ringshia RA, Legeros RZ, Clark E, Yost MJ, Terracio L, *et al.* An improved collagen scaffold for skeletal regeneration. *J Biomed Mater Res A*. 2010; 94(2): 371-379.
25. Valente J, Valente TAM, Alves P, Ferreira P, Silva A, Correia I. Alginate based scaffolds for bone tissue engineering. *Mater Sci Eng C*. 2012; 32(8): 2596-2603.
26. Kim J, Kim IS, Cho TH, Lee KB, Hwang SJ, Tae G, *et al.* Bone regeneration using hyaluronic acid-based hydrogel with bone morphogenic protein-2 and human mesenchymal stem cells. *Biomaterials*. 2007; 28(10): 1830-1837.
27. Park KH, Kim SJ, Lee WY, Song HJ, Park YJ. Hydrothermal fabrication and characterization of calcium phosphate anhydrous/chitosan composites. *Ceram Int*. 2017; 43(2): 2786-2790.
28. Prajatelista E, Lim C, Oh DX, Jun SH, Hwang DS. Chitosan and hydroxyapatite composite cross-linked by dopamine has improved anisotropic hydroxyapatite growth and wet mechanical properties. *Eng Life Sci*. 2015; 15(2): 254-261.
29. Suren UP, Israel OU, Ambalangodage JC. Injectable porous nano hydroxyapatite/chitosan/tripolyphosphate scaffolds with improved compressive strength for bone regeneration. *Mater Sci Eng C*. 2016; 69: 505-512.
30. Cai B, Zou Q, Zuo Y, Li L, Yang B, Li Y. Fabrication and cell viability of injectable n-HA/chitosan composite microspheres for bone tissue engineering. *RSC Adv*. 2016; 6(89): 85735-85744.
31. Azhar FF, Olad A, Salehi R. Fabrication and characterization of chitosan-gelatin/nanohydroxyapatite-polyaniline composite with potential application in tissue engineering scaffolds. *Des Monomers Polym*. 2014; 17(7): 654-667.
32. Nazeer MA, Yilgör E, Yilgör I. Intercalated chitosan/hydroxyapatite nanocomposites: Promising materials for bone tissue engineering applications. *Carbohydr Polym*. 2017; 175: 38-46.
33. Hanawa T, Davies J. In *The Bone-Biomaterial Interface* University of Toronto Press. 1991: 76.
34. Hench LL. Bioceramics: From concept to clinic. *J Am Ceram Soc*. 1991; 74(7): 1487-1510.
35. Reis R, Cunha A, Fernandes M, Correia R. Treatments to induce the nucleation and growth of apatite-like layers on polymeric surfaces and foams. *J Mater Sci Mater Med*. 1997; 8(12): 897-905.
36. Park SY, Perikamana SKM, Park JH, Kim SW, Shin H, Park SP, *et al.* Osteoinductive superparamagnetic Fe nanocrystal/calcium phosphate heterostructured microspheres. *Nanoscale*. 2017; 9(48): 19145-19153.
37. Duggan C, Watkins JB, Koletzko B, Walker WA. Nutrition in pediatrics: Basic science clinical applications. *Am J Clin Nutr*. 2016.
38. Gloria A, Russo T, d'Amora U, Zeppetelli S, d'Alessandro T, Sandri M, *et al.* Magnetic poly (ϵ -caprolactone)/iron-doped hydroxyapatite nanocomposite substrates for advanced bone tissue engineering. *J R Soc Interface*. 2013; 10(80): 20120833.

39. Iwasaki T, Nakatsuka R, Murase K, Takata H, Nakamura H, Watano S. Simple and rapid synthesis of magnetite/hydroxyapatite composites for hyperthermia treatments via a mechanochemical route. *Int J Mol Sci.* 2013; 14(5): 9365-9378.
40. Chandra VS, Baskar G, Suganthi RV, Elayaraja K, Joshy MIA, Beaula SW, *et al.* Blood compatibility of iron-doped nanosize hydroxyapatite and its drug release. *ACS Appl Mater Interfaces.* 2012; 4(3): 1200-1210.
41. Sneha M, Sundaram NM. Preparation and characterization of an iron oxide-hydroxyapatite nanocomposite for potential bone cancer therapy. *Int J Nanomedicine.* 2015; 10(1): 99-106.
42. Maurer J, Harris MM, Stanford VA, Lohman TG, Cussler E, Going SB, *et al.* Dietary iron positively influences bone mineral density in postmenopausal women on hormone replacement therapy. *J Nutr.* 2005; 135(4): 863-869.
43. Panseri S, Cunha C, D'Alessandro T, Sandri M, Giavaresi G, Marcacci M, *et al.* Intrinsically superparamagnetic Fe-hydroxyapatite nanoparticles positively influence osteoblast-like cell behaviour. *J Nanobio-technology.* 2012; 10(1): 1-10.
44. Zilm ME, Staruch M, Jain M, Wei M. An intrinsically magnetic biomaterial with tunable magnetic properties. *J Mater Chem.* 2014; 2(41): 7176-7185.
45. Iafisco M, Sandri M, Panseri S, Delgado-López JM, Gómez-Morales J, Tampieri A. Magnetic bioactive and biodegradable hollow Fe-doped hydroxyapatite coated poly (L-lactic) acid micro-nanospheres. *Chem Mater.* 2013; 25(13): 2610-2617.
46. Radha G, Venkatesan B, Rajashree P, Vellaichamy E, Balakumar S. Insights into the apatite mineralization potential of thermally processed nanocrystalline Ca_{10-x}Fe_x(PO₄)₆(OH)₂. *New J Chem.* 2019; 43(3): 1358-1371.
47. Singh YP, Dasgupta S, Bhaskar R. Preparation, characterization and bioactivities of nano anhydrous calcium phosphate added gelatin-chitosan scaffolds for bone tissue engineering. *J Biomater Sci Polym Ed.* 2015; 30(18):1756-1778.
48. Rahman MS, Rana MM, Spitzhorn LS, Akhtar N, Hasan MZ, Choudhury N, *et al.* Fabrication of biocompatible porous scaffolds based on hydroxyapatite/collagen/ chitosan composite for restoration of defected maxillofacial mandible bone. *Prog Biomater.* 2019; 8(3): 137-154.
49. Yang J, Long T, He NF, Guo YP, Zhu ZA, Ke QF. Fabrication of a chitosan/bioglass three-dimensional porous scaffold for bone tissue engineering applications. *J Mater Chem B.* 2014; 2(38): 6611-6618.
50. Baxter LC, Frauchiger V, Textor M, Ap Gwynn I, Richards RG. Fibroblast and osteoblast adhesion and morphology on calcium phosphate surfaces. *Eur Cells Mater.* 2002; 4(1) :1-7.
51. Tagaya M, Ikoma T, Takemura T, Migita S, Okuda M, Yoshioka T, *et al.* Initial adhesion behavior of fibroblasts onto hydroxyapatite nano-crystals. *Bioceram Dev Appl.* 2011; 1: 1-4.
52. Heidari F, Razavi M, Bahrololoom ME, Bazargan-Lari R, Vashae D, Kotturi H, *et al.* Mechanical properties of natural chitosan/hydroxyapatite/magnetite nano-composites for tissue engineering applications. *Mater Sci Eng C.* 2016; 65: 338-344.
53. Li Z, Ramay HR, Hauch KD, Xiao D, Zhang M. Chitosan-alginate hybrid scaffolds for bone tissue engineering. *Biomaterials.* 2005; 26(18): 3919-3928.
54. Aslani M, Meskinfam M, Aghabozorg HR. In situ biomimetic synthesis of gelatin-carbon nanotube-hydroxyapatite biocomposites as bone filler. *Orient J Chem.* 2017; 33(1): 235-241.
55. Shahabi S, Najafi F, Majdabadi A, Hooshmand T, Haghbin Nazarpak M, Karimi B, *et al.* Effect of gamma irradiation on structural and biological properties of a PLGA-PEG-hydroxyapatite composite. *Sci World J.* 2014.